https://doi.org/10.5194/essd-2024-589
Preprint. Discussion started: 30 January 2025

A high-resolution divergence and vorticity dataset in Beijing derived from the radar wind profiler mesonet measurements

Xiaoran Guo[a], Jianping Guo[a], Deli Meng[a], Yuping Sun[a], Zhen Zhang[a,b], Hui Xu[a], Liping Zeng[c], Juan Chen[d], Ning Li[a], Tianmeng Chen[a]

[a]State Key Laboratory of Severe Weather, Chinese Academy of Meteorological Sciences, Beijing 100081, China

[b]Department of Atmospheric and Oceanic Sciences & Institute of Atmospheric Sciences, Fudan University, Shanghai 200438, China

[c]Guizhou New Meteorological Technology Co., Ltd, Guiyang 550001, China

[d]AVIC Leihua Electonic Technology Research Institute, Wuxi 214063, China

Correspondence to:

Prof. Jianping Guo (Email: jpguocams@gmail.com)

https://doi.org/10.5194/essd-2024-589
Preprint. Discussion started: 30 January 2025

Abstract

Low-level convergence and cyclonic circulation are one of the most important dynamic variables in governing the initiation and development of convective storms. Our ability to obtain high-resolution horizontal divergence and vertical vorticity profiles, nevertheless, remains limited largely due to the lack of vertical wind observations. To fill this data gap, a high-density mesonet consisting of six radar wind profilers (RWP) sites has been operated in Beijing, which allowed for continuous observations of the three-dimensional winds with high vertical resolution. This paper aims to produce a temporally continuous horizontal divergence and vertical vorticity dataset at the vertical resolution of 120 m, which are derived from horizontal winds measured by the RWP mesonet in Beijing by using the triangle method. This dataset is generated at intervals of 6-minute for the whole year of 2023, covering the altitude range of 0–5 km. The dynamic variables from RWP mesonet are found to scatter sharply, as opposed to those from ERA5 that are concentrated around zero, especially at the high altitudes. Particularly, the negative divergence and positive vorticity are detected in the low-level troposphere up to 1 h in advance of the occurrence of rainfall events, and their magnitudes are increasingly becoming greater when the time comes closer to the rainfall onset, exhibiting the key role that the dataset plays in rainfall nowcasting. This is indicative of, to some extent, the effectiveness of high-resolution divergence and vorticity dataset in Beijing. The dataset is publicly available at https://doi.org/10.5281/zenodo.14176969 (Guo et al., 2024a), which is of significance for a multitude of scientific research and applications, including convection initiation, air quality forecasting, among others. Therefore, the findings highlight the urgent need of exploiting the dynamic variables from the RWP mesonet measurements to better characterize the pre-storm environment.

https://doi.org/10.5194/essd-2024-589
Preprint. Discussion started: 30 January 2025

Open Access Earth System Science Data Discussions

Short Summary

Optimal atmospheric dynamic condition is essential for convective storms. This study generates a dataset of high-resolution divergence and vorticity profiles using the measurements of radar wind profiler mesonet in Beijing. The negative divergence and positive vorticity are present in advance of rainfall events. This suggests that this dataset can help improve our understanding of prestorm environment and has the potential to be applied to weather forecasting.

1. Introduction

Atmospheric dynamic conditions, such as vorticity, divergence, and vertical velocity, play a critical role in inferring convection initiation (CI) and the subsequent development of mesoscale convective systems (MCSs) (Ulanski and Garstang, 1978; Weckwerth and Parsons 2006; Wilson and Roberts 2006; Lock and Houston 2014; Weckwerth et al., 2019; Guo et al., 2024b). In recent decades, a variety of previous observational analysis based on passive surface station and weather radar reveal the positive correlation between surface convergence and the formation of new convective cells (Purdom 1976; Fankhauser et al., 1995; Kalthoff et al., 2009; Bai et al., 2019). The sustained and enhanced updraft forced by local convergence is conducive to the initiation or intensification of convective cells, especially in unstable and deep moist environments. Furthermore, the interaction between wind shear and vertical vorticity structure produces favorable atmospheric conditions for cyclogenesis in both midlatitude and tropical regions during the warm season (Bosart and Sanders, 1981; Zhang and Fritsch, 1987). The pressure drop caused by the cyclonic rotation of the low-level mesocyclone further accelerates the lifting, as described by the mesoscale vertical vorticity equation used in vertical velocity analyses (Yanai and Nitta, 1967; Brandes and Ziegler, 1993, Shapiro et al., 2009).

https://doi.org/10.5194/essd-2024-589
Preprint. Discussion started: 30 January 2025

Additionally, the radiosonde sounding arrays have been used to obtain the vertical wind profiles that are further applied for retrievals of atmospheric dynamic variables over large spatial scales exceeding 500 km. In this case, the wind gradients are objectively determined by the linear interpolation to grid points using observations of distant stations with inevitable errors (Lee and Browning, 1993). Afterwards, many follow-on studies confirmed its possibility to realistically calcualte the mass divergence of the air over an area by using soundings or dropsondes distributed along the perimeter of this area (e.g., Holland and Rasmusson, 1973; Nitta and Esbensen, 1974; Lenschow et al.,1999, 2017). On the other hand, vertical vorticity can be directly determined from Stokes theorem using closed integrals of the horizontal velocity tangent component enclosing the area. For instance, Davies-Jones (1993) investigated the algorithms to estimate vertical vorticity profiles and associated errors over sub-synoptic scale regions from a small number of observing stations. During an airborne field campaign over the tropical Atlantic near Barbados, the dropsondes with horizontal wind profile measurements were released with high frequency along circular flight patterns to estimated vertical profiles of the area-averaged mass divergence and vorticity (Bony and Stevens, 2019). Nevertheless, it is proved that the triangle method is more practical in operation if observations are irregularly distributed (Bellamy, 1949).

Nowadays, divergence and vorticity over smaller areas, with linear dimensions on the order of 100 km, have attracted widespread attention due to the importance of mesoscale vertical motions (Bony et al., 2017). With the advent of dense remote sensing instruments, more accurate retrievals of divergence and vorticity profiles are more possible due to wind fields with higher precision and resolution. A new generation of ground-based radar wind profiler (RWP) network has been operated in China as of 2008 (Guo et al., 2021), which consists of over 260 stations by the end of 2023. It has good spatial coverage with six RWP sites over the Beijing metropolitan region (BMR), which provide continuous observations of high-resolution three-dimensional wind fields (Liu et al., 2019; Guo et al., 2023). In our previous study (e.g.,

https://doi.org/10.5194/essd-2024-589
Preprint. Discussion started: 30 January 2025

Open Access Earth System Science Data Discussions

Guo et al, 2023, 2024b; Chen et al., 2024), the vertically resolved dynamic parameters were calculated from the measurements of RWP mesonet to identify the pre-storm conditions and forecast the ensuing evolution of MCSs.

In the present study, a long-term horizontal divergence and vertical vorticity dataset covering the whole year of 2023 are generated, which have crucial implications for the identification and evaluation of vertical motion and convection development. The rest of the paper is organized as follows. Section 2 describes the fundamental data sets and the calculation methodology used here. A comparison analysis is conducted of dynamic variable profiles between RWPs retrieval and ERA5 reanalysis in Section 3. Sections 4 represented the variation patterns of these two dynamic parameters preceding rainfall events. Main conclusions are given in the final section.

2. Data and Methodology

2.1 Radar wind profiler measurements

Figure 1 presents the BMR's RWP mesonet, which consists of six RWPs deployed at the following stations: Huairou (HR; 40.36°N, 116.63°E), Yanqing (YQ; 40.45°N, 115.97°E), Shangdianzi (SDZ; 40.66°N, 117.11°E), Pinggu (PG; 40.17°N, 117.12°E), Haidian (HD; 39.98°N, 116.28°E), and the Beijing Weather Observatory (BWO). The RWP mesonet provides measurements of horizontal and vertical winds, and refractive index structure parameter at 6-min intervals. The vertical resolution is 120 m below 4 km above the ground level (AGL) in low-operating mode, and 240 m from 4 to 10 km AGL in high-operating mode (Liu et al., 2019). According to the validation results against radiosonde measurements in BWO by Guo et al. (2023), the horizontal winds derived from RWPs in the altitude range of 0.5–5km above the ground level (AGL) spanning a whole year of 2023 are believed to be reliable enough and then be adopted here for the generation of atmospheric dynamic dataset.

https://doi.org/10.5194/essd-2024-589
Preprint. Discussion started: 30 January 2025

Open Access Earth System Science Data Discussions

2.2 Calculation of horizontal divergence and vertical vorticity

By applying the Gauss's theorem, horizontal divergence D is expressed by the relative expansion rate of the air mass. The triangle method, as proposed by Bellamy (1949), computes the divergence based on the rate of change in a fluid triangle initially coincident with the network composed by any three points *A, B,* and *C.* We assume that $(x_i, y_i)\ (i = 1,2,3)$ are the location of three vortex points, $(u_i, v_i)\ (i = 1,2,3)$ are the zonal and meridional component of horizontal wind, respectively. As the air parcel at $(x_i, y_i)\ (i = 1,2,3)$ moves to $(x_i + u_i\Delta t, y_i + v_i\Delta t)$ after the infinitesimally short time Δt, a new triangle $A^{'}B^{'}C^{'}$ will form. The resultant horizontal divergence D over the fluid triangle can be defined as

$$D = \frac{1}{\sigma}\frac{d\sigma}{dt} = \frac{1}{\sigma}\lim_{\Delta t \to 0}\frac{\Delta\sigma}{\Delta t} = \frac{1}{\sigma}\lim_{\Delta t \to 0}\frac{\sigma^{'} - \sigma}{\Delta t} \tag{1}$$

where σ and σ' denote the area of the triangle ABC and $A^{'}B^{'}C^{'}$, which can be formulated by

$$\sigma = \frac{1}{2}(\overrightarrow{AB} \times \overrightarrow{AC}) \cdot \vec{k} = \frac{1}{2}\begin{vmatrix} \vec{i} & \vec{j} & \vec{k} \\ x_2 - x_1 & y_2 - y_1 & 0 \\ x_3 - x_1 & y_3 - y_1 & 0 \end{vmatrix} \cdot \vec{k} \tag{2}$$

$$\sigma^{'} = \frac{1}{2}\begin{vmatrix} \vec{i} & \vec{j} & \vec{k} \\ (x_2 + u_2\Delta t) - (x_1 + u_1\Delta t) & (y_2 + v_2\Delta t) - (y_1 + v_1\Delta t) & 0 \\ (x_3 + u_3\Delta t) - (x_1 + u_1\Delta t) & (y_3 + v_3\Delta t) - (y_1 + v_1\Delta t) & 0 \end{vmatrix} \cdot \vec{k} \tag{3}$$

Here, $\vec{i}$, $\vec{j}$, $\vec{k}$ represent the unit vectors of zonal, meridional and the vertical axis in the coordinate system, respectively. Substituting Eqs. (3) and (2) into Eq. (1) and simplifying, the triangle-area averaged horizontal divergence is as follows

$$D = \frac{(u_2 - u_1)(y_3 - y_1) - (u_3 - u_1)(y_2 - y_1) + (x_2 - x_1)(v_3 - v_1) - (x_3 - x_1)(v_2 - v_1)}{(x_2 - x_1)(y_3 - y_1) - (x_3 - x_1)(y_2 - y_1)} \tag{4}$$

The vertical vorticity ζ can be estimated directly from Stokes theorem as

$$\zeta = \frac{1}{\sigma}\oint \vec{V} \cdot d\vec{r} \tag{5}$$

https://doi.org/10.5194/essd-2024-589
Preprint. Discussion started: 30 January 2025

Circulation along the triangle $\boldsymbol{ABC}$ can be calculated by

$$\oint \vec{V} \cdot d\vec{r} = \frac{(\vec{V_1}+\vec{V_2})\cdot\overrightarrow{AB}}{2} + \frac{(\vec{V_2}+\vec{V_3})\cdot\overrightarrow{BC}}{2} + \frac{(\vec{V_3}+\vec{V_1})\cdot\overrightarrow{CA}}{2} \tag{6}$$

where $\vec{V_i} = (u_i, v_i)(i = 1, 2, 3)$ is the vector of the horizontal wind at $\boldsymbol{A}$, $\boldsymbol{B}$, and $\boldsymbol{C}$. Substituting Eqs. (2) and (6) into Eq. (5), the vertical vorticity is as follows

$$\zeta = \frac{(v_2 - v_1)(y_3 - y_1) - (v_3 - v_1)(y_2 - y_1) - (x_2 - x_1)(u_3 - u_1) + (x_3 - x_1)(u_2 - u_1)}{(x_2 - x_1)(y_3 - y_1) - (x_3 - x_1)(y_2 - y_1)} \tag{7}$$

These equations are then applied to the above-mentioned wind measurements from the RWP mesonet in order to calculate the profile of horizontal divergence and vertical vorticity. Four triangles from west to east are constructed based on the position of RWP stations in the BMR. Considering the six RWPs located at different terrain elevations, the horizontal velocities measured by each RWP are interpolated to the same altitude that starts upwards from 0.51 km to 4.95 km above mean sea level (AMSL) with a vertical resolution of 120 m.

2.3 Rain Gauge Measurements and ERA5 reanalysis

Rainfall at 1-min interval is directly acquired from the rain gauge measurements at automated surface stations over Beijing. Here, 6-min accumulated rainfall is synchronized with the RWP measurements at 6-min interval. These rain gauge measurements have undergone rigorous quality control and are publicly available by the China Meteorological Administration.

ERA5 is the fifth-generation atmospheric reanalysis of ECMWF (European Centre for Medium-Range Weather Forecasts), which benefits from advancements in data assimilation, model physics and dynamics (Hersbach et al., 2020). ERA5 dataset can provide divergence and vorticity on 37 pressure level with a spatial resolution of 0.25°×0.25° at hourly intervals. Additionally, the planetary boundary layer (PBL) height product is directly obtained from the ERA5 reanalysis.

https://doi.org/10.5194/essd-2024-589
Preprint. Discussion started: 30 January 2025

3. Comparison analysis of dynamic variables from RWP with those from ERA5

Due to the widespread usage of ERA5 reanalysis in characterizing stable condition of atmosphere, evaluating its performance in representing the vertical profiles becomes crucial. The divergence and vorticity fields derived from the RWP mesonet are compared with ERA5 reanalysis in the non-precipitation day in this section. To match the spatial resolution of the ERA5 dataset on the grid of 0.25°× 0.25° to the RWP mesonet, divergence and vorticity profiles of all the grids within this triangle are averaged for each triangle. Simultaneously, observed profiles at 1-hour interval are applied in accordance with the temporal resolution of reanalysis.

It is well known that the PBL is the lowermost part of the troposphere that governs the exchange of momentum, mass and heat between surface and atmosphere. There are significant differences between the wind field in the PBL and the upper atmosphere. To better reveal the characteristics of divergence and vorticity at different heights, the sum of the average elevation and PBL height are defined as z_i. The altitude is normalized by z_i to provide a nondimensional vertical coordinate for horizontal divergence and vertical vorticity. The criterion of z/z_i is set as 1 and 2 to separate different altitude layers to near-surface, low-level, and midlevel layer for the following analyses. Figure 2 shows the normal distribution of two dynamic parameters derived from RWPs mesonet and ERA5 reanalysis for all non-precipitation day in 2023. Overall, the distributions of observed parameters on the different altitude layer are similar. The value of divergence and vorticity by ERA5 reanalysis are more significantly concentrated in zero, indicating that the ERA5 reanalysis underestimates the amplitude compared with the RWPs mesonet measurements. The higher peak probability is found in the low-level and midlevel troposphere. This illustrates that ERA5 reanalysis does not detect well divergence and vorticity at higher altitudes, which resembles the results in previous studies (Taszarek

https://doi.org/10.5194/essd-2024-589
Preprint. Discussion started: 30 January 2025

et al., 2021; Wu et al., 2024). We speculate the difference may be likely resulted from insufficient wind profiling measurements in China being assimilated into ERA models.

To further explore the overall differences of vertical profiles between reanalysis datasets and observation more quantitatively, divergence and vorticity from RWPs mesonet measurements are validated against ERA5 after interpolating the reanalysis to corresponding level. As shown in Figure 3a-c, ERA5 reanalysis cannot characterize the potential horizontal and vertical motion in a non-precipitation environment with the correlation coefficient (R) less than 0.1. It's also evident that ERA5 exhibits a substantial underestimation of divergence, especially at the higher altitudes. Noteworthy is that ERA5 reanalysis exhibits better performance in representing vertical vorticity with R reaching 0.3 even though the disparity is still apparent (Figure 3d-f). This could be due to the magnitude of vorticity being greater than that of divergence.

4. Height-resolved temporal patterns of dynamic variables preceding the onset of rainfall

The ERA5 reanalysis with lower temporal resolution is recognized to have limited capability of characterizing the temporally continuous evolution of atmospheric motion in a pre-storm environment over a mesoscale region. It is desirable to fill this gap with height-resolved dynamic variables as calculated with the RWP mesonet measurements at 6-min intervals. In this section, we attempt to explore how the horizontal divergence and vertical vorticity derived from the RWP mesonet could be used as precursors for the pre-storm environment conditions. The triangle-area-averaged rainfall amount (mm), which is obtained from 29, 42, 49, and 15 rain gauges in triangles 1, 2, 3, and 4 respectively, is used to identify rainfall events occurring during the whole year of 2023 over the BMR's RWP mesonet. For each triangle, all rainfall moments are selected when the 6 min accumulated triangle-area-averaged rainfall is greater than zero. Considering the intermittent nature of rainfall, all the adjacent rainfall events being separated by less than 2 hours are classified as the same rainfall event. That's to say, the interval between two rainfall events is

https://doi.org/10.5194/essd-2024-589
Preprint. Discussion started: 30 January 2025

required to be at least 2 hours. The first and last rainfall moment of every rainfall event are defined as the occurrence and ending time of rainfall event, respectively. To avoid the impact of data error, the rainfall events with duration of less than 30 minutes are discarded. Finally, a total of 462 rainfall events are identified over the RWP mesonet in 2023.

Figure 4a and 4b present the normalized contoured frequency by altitude (NCFAD) for all profiles of the horizontal divergence and vertical vorticity as observed by the RWP mesonet within 1-hour preceding rainfall events, respectively. The pre-storm dynamic environment exhibits significant difference, which implies the presence of complex vertical motion in this unstable atmosphere. By using dynamic parameters with higher temporal resolution obtained from the RWPs mesonet, our aim is to further explore potential patterns or trends in the pre-rainfall convection environment during the lead time. Figures 5a and 5b show the evolutions of average profiles of horizontal divergence and vertical vorticity at 12-min interval before the occurrence of rainfall events.

Specifically, the horizontal divergence with maximum frequency appears about 0 above 1 km AMSL (Figure 4a). In contrast, the divergence below 1 km AMSL significantly concentrates from -5×10^{-5} s^{-1} to 0. The presence of weak convergence, as indicated by negative value of divergence, is possibly associated with topography. In spite of this weaknesses, convergence tends to provide favorable upward motions in the lower troposphere. These upward motions represent the important lifting of moist air near surface that facilitates the subsequent formation of clouds and onset the convective rainfall. Typically, Wilson and Schreiber (1986) extensively elucidated the potential precursors of convergent processes in the PBL to CI and intensifying existing storms by providing locally enhanced updrafts. The significant increase in average convergence below 1.5 km AMSL within 48 min ahead of precipitation (Figure 5a) is largely contributed to the fact that near-surface air tends to strongly converge into the pre-squall mesotrough when the system approaches. The main convection was collocated with low-level convergence and midlevel divergence

https://doi.org/10.5194/essd-2024-589
Preprint. Discussion started: 30 January 2025

placed ahead of the precipitation center. These patterns are consistent with previous studies (Zhang et al., 1989; Qin and Chen, 2017; Yin et al., 2020).

As indicated in Figure 4b, the magnitude of vorticity is greater than that of divergence with more vertical fluctuation in the lower to mid-troposphere. The lowest layer is dominated by positive vorticity centering near 1 km AMSL. Similarly, the significant increase in vertical vorticity shown in Figure 5b might be in part attributed to the preexisting ambient vorticity associated with significant horizontal wind shear. The environmental wind field before the arrival of MCS is critical to system organization since the orientation of its vertical shear directly influences an asymmetric precipitation structure with mesoscale rotation. In addition, the mesoscale convectively vortex (MCV) may be resulted from deep and moist convection prior to the passage of the MCS (Wang et al. 1993). Trier et al. (1997) indicated that the MCS-induced horizontal flow and its associated vertical shear are critical factors which influence the development of the vortex. This southwesterly flow, enhanced by the by the MCV circulation, transports moisture northward in the lower troposphere, thereby creating potential instability ahead of the vortex center. Such an environment is favorable for convection and further lead heavy precipitation (Johnson et al., 1989; Hendricks et al., 2004; Lai et al., 2011).

5. Concluding remarks and summary

The generation and organization of convergence and rotation are the recurring theme of baroclinic convection in midlatitude during the warm season. Owing to relatively few direct observations, the detailed structure of MCSs has not been exactly explored. The unique aspect of this study is the analysis of the enhanced observations derived from the new-generation ground-based RWP mesonet in Beijing. The RWP mesonet is shown being capable of continuously observing the horizontal wind fields in the lower troposphere with ultra-high vertical and temporal resolutions. The horizontal wind measurements are then used to calculate the vertical profiles of the

https://doi.org/10.5194/essd-2024-589
Preprint. Discussion started: 30 January 2025

triangle-area-averaged horizontal divergence and vertical vorticity, which is well indicative of the dynamic structure in the lower to mid-troposphere.

Compared to the vertical profiles with higher accuracy, ERA5 exhibits a substantial underestimation of divergence and vorticity, especially at the higher altitudes. ERA5 reanalysis cannot characterize the potential horizontal and vertical motion even in a non-precipitation environment. The limitation may be likely due to the lack of higher-level wind profiling measurements in China being assimilated into ERA models. In addition, ERA5 reanalysis is unable to identify the propagation of MCSs and provide the real-time precursor signals of precipitation. The RWP-derived convergence and cyclonic circulation can provide useful information with a temporal resolution of 6-minute for detecting rainfall initiation, which filling the gap of sounding and reanalysis for nowcasting the occurrence of rainfall events.

For this purpose, a statistical analysis of the vertical divergence and vorticity profiles preceding rainfall events over the RWP mesonet in 2023 are performed. Results show that the patterns of increasing low-level convergence and cyclonic circulation is evident before the occurrence of rainfall events. This indicates the development of the corresponding upward motion, at least in the lower troposphere, prior to the arrival the passage of the storm, respectively. The convergence near surface, in combination with the low-level cyclonic rotation, provide favorable dynamic conditions to lift moist air for the subsequent formation of clouds and onset the convective rainfall.

In conclusion, the RWP mesonet can be used to calculate the vertical profiles of divergence and vorticity in the lower to mid-troposphere more realistically compared to reanalysis dataset. These dynamic variables from observations can provide useful information for characterizing the process of convection and detecting rainfall initiation in advance. While the results presented above are encouraging, it is imperative to fill the observational gaps near surface and apply them to nowcasting of severe weather events as well as the improvement of initial conditions in numerical weather prediction models. Furthermore, the orographic influence on the structure of the convergence, vortex and precipitation will also be explored in a forthcoming study.

Author contributions

JG designed the research framework and conceptualized this study; XG and JG conducted the experiment and drafted the initial manuscript; TC and NL helped the data collection and carried out the quality control. LZ, JC, FZ and YS contributed to the revision of the manuscript. All authors participated in result interpretation.

Competing interests

The contact author has declared that there are no competing interests for all authors.

Financial support

This manuscript was jointly under the auspices of the National Natural Science Foundation of China under grants of 42325501, the Chinese Academy of Meteorological Sciences under grant 2024Z003 and the Department of Science and Technology of Guizhou province under grant KXJZ [2024] 033.

Data availability

The divergence and vorticity dataset over Beijing can be accessed at https://doi.org/10.5281/zenodo.14176969 (Guo et al., 2024a). We are grateful to ECMWF for providing ERA5 hourly data, which are available at https://www.ecmwf.int/en/forecasts/datasets/reanalysis-datasets/era5/. The meteorological measurements of automatic weather stations are obtained from the National Meteorological Information Center of China Meteorological Administration (https://data.cma.cn) via registration.

https://doi.org/10.5194/essd-2024-589
Preprint. Discussion started: 30 January 2025

References

Bai, L., Meng, Z., Huang, Y., Zhang, Y., Niu, S., and Su, T.: Convection initiation resulting from the interaction between a quasi-stationary dryline and intersecting gust fronts: A case study, *Journal of Geophysical Research: Atmospheres*, 124, 2379–2396. https://doi.org/10.1029/2018JD029832, 2019.

Bellamy, J.C.: Objective calculations of divergence, vertical velocity and vorticity, *Bull. Amer. Meteor. Soc.*, 30, 45-49, https://doi.org/10.1175/1520-0477-30.2.45, 1949.

Bony, S., Stevens, B., Ament, F., and Coauthors: EUREC^{4}A: A field campaign to elucidate the couplings between clouds, convection and circulation, *Surv. Geophys.*, 38, 1529–1568, https://doi.org/10.1007/s10712-017-9428-0, 2017.

Bony, S., and Stevens, B.: Measuring area-averaged vertical motions with dropsondes, *J. Atmos. Sci.*, 76, 767-783, https://doi.org/10.1175/JAS-D-18-0141.1, 2019.

Bosart, L. F., and Sanders, F.: The Johnstown flood of July 1977: A long-lived convective storm, *J. Atmos. Sci.*, 38(8), 1616 – 1642, doi: 10.1175/1520-0469(1981)038<1616:TJFOJA>2.0.CO;2, 1981.

Brandes, E. A., and Ziegler, C. L.: Mesoscale downdraft influences on vertical vorticity in a mature mesoscale convective system, *Mon. Wea. Rev.*, 121, 1337-1353, https://doi.org/10.1175/1520-0493(1993)121<1337:MDIOVV>2.0.CO;2, 1993.

Chen, T., Guo, J., Guo, X., Zhang, Y., Xu, H., and Zhang, D.-L: On the multiscale processes leading to an extreme gust wind event in East China: Insights from radar wind profiler mesonet observations. *Journal of Geophysical Research: Atmosphere*, 129, https://doi.org/10.1029/2024JD041484, 2024.

Davies-Jones, R.: Useful, formulas for computing divergence, vorticity, and their errors from three or more stations, *Mon. Wea. Rev.*, 121: 713-725, 1993.

Fankhauser, J. C., Crook, N. A., Tuttle, J., and Coauthors: Initiation of Deep

https://doi.org/10.5194/essd-2024-589
Preprint. Discussion started: 30 January 2025

Convection along Boundary Layer Convergence Lines in a Semitropical Environment, *Mon. Wea. Rev.*, **123**(2), 291-314, 1995.

Guo, J., Liu, B., Gong, W., Shi, L., Zhang, Y., Ma, Y., Zhang, J., Chen, T., Bai, K., Stoffelen, A., de Leeuw, G., and Xu, X.: Technical note: First comparison of wind observations from ESA's satellite mission Aeolus and ground-based radar wind profiler network of China, *Atmos. Chem. Phys.*, **21,** 2945–2958, https://doi.org/10.5194/acp-21-2945-2021, 2021.

Guo, J., Guo, X.: A temporally continuous divergence and vorticity dataset in Beijing derived from the radar wind profiler mesonet during 2023 [Data set], https://doi.org/10.5281/zenodo. 14176969, 2024a.

Guo, X., Guo, J., Zhang, D-L., and Yun, Y: Vertical divergence profiles as detected by two wind profiler mesonets over East China: implications for nowcasting convective storms, *Q. J. R. Meteorol. Soc.*, 149(754), 1629-1649, doi:10.1002/qj.4474, 2023.

Guo, X., Guo, J., Chen, T., Li, N., Zhang, F., and Sun, Y.: Revisiting the evolution of downhill thunderstorms over Beijing: a new perspective from a radar wind profiler mesonet, *Atmos. Chem. Phys.*, 24, 8067–8083, https://doi.org/10.5194/acp-24-8067-2024, 2024b.

Hendricks, E. A., Montgomery, M. T., Davis, C. A.: On the role of "vortical" hot towers in formation of tropical cyclone Diana, *J Atmos Sci*, 61, 1209-1232. https://doi.org/10.1175/1520-0469(2004)061<1209:TROVHT>2.0.CO;2, 2004

Hersbach, H., Bell, B., Berrisford, P., and Coauthors: The ERA5 global reanalysis, *Q. J. R. Meteorol. Soc.*, 146(730), 1999–2049, https://doi.org/10.1002/qj.3803, 2020.

Holland, J. Z.: Preliminary report on the BOMEX sea-air interaction program, *Bull. Amer. Meteor. Soc.*, 51, 809 – 820, https://doi.org/10.1175/1520-0477(1970)051,0809:PROTBS.2.0.CO;2, 1970.

Johnson, R. H., Chen, S., Toth, J. J.: Circulations associated with a mature-to-decay midlatitude mesoscale convective system. Part I: Surface features-heat bursts and mesolow development, *Mon. Wea. Rev.*, 117(5), 942-959,

https://doi.org/10.5194/essd-2024-589
Preprint. Discussion started: 30 January 2025

https://doi.org/10.1175/1520-0493(1989)117<0942:CAWAMT>2.0.CO;2, 1989.

Kalthoff, N., Adler, B., Barthlott, C., and Coauthors: The impact of convergence zones on the initiation of deep convection: A case study from COPS, *Atmos. Res.* 93(4): 680-694, 2009.

Lai, H. W., Davis, C. A., Jou, B. J.-D.: A subtropical oceanic mesoscale convective vortex observed during SoWMEX/TiMREX, *Mon. Wea. Rev.*, 139(8), 2367-2385, https://doi.org/10.1175/2010MWR3411.1, 2011.

Lee, J. L., and Browning, G. L.: Analysis of Errors in the Horizontal Divergence Derived from High Temporal Resolution of the Wind, *Mon. Wea. Rev.*, 122(5), 851-863, doi: 10.1175/1520-0493(1994)1222.0.CO;2, 1993.

Lenschow, D. H., Krummel, P. B., and Siems, S. T.: Measuring entrainment, divergence, and vorticity on the mesoscale from aircraft, *J. Atmos. Oceanic Technol.*, 16, 1384 – 1400, https://doi.org/10.1175/1520-0426(1999)016,1384:MEDAVO.2.0.CO;2, 1999.

Lenschow, D. H., Savic-Jovcic, V., and Stevens, B.: Divergence and vorticity from aircraft air motion measurements, *J. Atmos. Oceanic Technol.*, 24, 2062–2072, https://doi.org/10.1175/2007JTECHA940.1, 2007.

Liu, B., Ma, Y., Guo, J., and Coauthors: Boundary layer heights as derived from ground-based radar wind profiler in Beijing, *IEEE Transactions on Geoscience and Remote Sensing*, 57, 8095-8104, https://doi.org/10.1109/TGRS.2019.2918301, 2019.

Lock, N. A., and Houston, A. L.: Empirical examination of the factors regulating thunderstorm initiation, *Mon. Wea. Rev.*, **142**, 240-258, https://doi.org/10.1175/MWR-D-13-00082.1, 2014.

Nitta, T., and Esbensen, S.: Heat and moisture budget analyses using BOMEX data, *Mon. Wea. Rev.*, 102, 17-28, https://doi.org/10.1175/1520-0493(1974)102,0017:HAMBAU.2.0.CO;2, 1974.

Purdom, J. F. W.: Some uses of high-resolution GOES imagery in the mesoscale forecasting of convection and its behavior, *Mon. Wea. Rev.*, **104**, 1474–1483,

https://doi.org/10.5194/essd-2024-589
Preprint. Discussion started: 30 January 2025

https://doi.org/10.1175/1520-0493(1976)1042.0.CO;2, 1976.

Qin, R., and Chen, M.: Impact of a front–dryline merger on convection initiation near a mountain ridge in Beijing, *Mon. Wea. Rev.*, 145, 2611-2633, https://doi.org/10.1175/MWR-D-16-0369.1, 2017).

Shapiro, A., Potvin, C. K., and Jidong, G.: Use of a vertical vorticity equation in variational dual-Doppler wind analysis, *J. Atmos. Oceanic Technol.*, 26, 2089–2106, 2009.

Taszarek, M., Pύcik, T., Hoogewind, K., Allen, J.T., and Coauthors: Comparison of convective parameters derived from ERA5 and MERRA-2 with rawinsonde Data over Europe and North America, *J. Climate*, 34(8), 3211–3237, 2021.

Trier, S. B., Skamarock, W. C., and LeMone, M. A.: Structure and evolution of the 22 February 1993 TOGA Squall Line: Organization Mechanisms Inferred from Numerical Simulation, *J. Atmos. Sci.*, 54(3), 386-407, https://doi.org/10.1175/1520-0469(1997)054<0386:SAEOTF>2.0.CO;2, 1997.

Ulanski, S. L., and Garstang, M.: The role of surface divergence and vorticity in the life cycle of convective rainfall. Part I: Observations and analysis, *J. Atmos. Sci.*, **35**, 1047–1062, https://doi.org/10.1175/1520-0469(1978)035<1063:TROSDA>2.0.CO;2, 1978.

Wang, W., Kuo, Y. H., and Warner, T. T.: A diabatically driven mesoscale vortex in the lee of the Tibetan Plateau, Mon. Wea. Rev., 121, 2542–2561, 1993.

Weckwerth, T. M., and Parsons, D. B.: A review of convection initiation and motivation for IHOP 2002, *Mon. Wea. Rev.*, **134**, 5-22, https://doi.org/10.1175/MWR3067.1, 2006.

Wilson, J.W., and Schreiber, W.E.: Initiation of convective storms at radar-observed boundary-layer convergence lines, *Mon. Wea. Rev.*, 114, 2516-2536, https://doi.org/10.1175/1520-0493(1986)114<2516:iocsar>2.0.co;2, 1986.

Wilson, J.W., and Roberts, R.D.: Summary of convective storm initiation and evolution during IHOP: Observational and modeling perspective, *Mon. Wea.*

https://doi.org/10.5194/essd-2024-589
Preprint. Discussion started: 30 January 2025

Rev., **134**, 23-47, https://doi.org/10.1175/MWR3069.1, 2006.

Weckwerth, T. M., Hanesiak, J., Wilson, J. W., and Coauthors: Nocturnal convection initiation during PECAN 2015, *Bull. Amer. Meteor. Soc.*, **100**, 2223-2239, https://doi.org/10.1175/BAMS-D-18-0299.1, 2019.

Wu, J., Guo, J., Yun, Y., and Coauthors: Can ERA5 reanalysis data characterize the pre-storm environment? *Atmospheric Research*, 297, 107108, https://doi.org/10.1016/j.atmosres.2023.107108, 2023.

Yanai, M., and Nitta, T.: Computation of vertical motion and vorticity budget in a Caribbean easterly wave, *J. Meteor. Soc. Japan*, 45, 444–466, 1967.

Yin, J., Zhang, D.-L., Luo, Y., and Ma, R.: On the extreme rainfall event of 7 May 2017 over the coastal city of Guangzhou. Part I: Impacts of urbanization and orography, *Mon. Wea. Rev.*, 148, https://doi.org/10.1175/MWR-D-19-0212.1, 2020.

Zhang, D. L., and Fritsch, J. M.: Numerical simulation of the Meso-β scale structure and evolution of the 1977 Johnstown flood. Part II: Inertially stable warm-core vortex and the mesoscale convective complex, *J. Atmos. Sci.*, 43(18):1913-1944, doi: 10.1175/1520-0469(1986)043<1913:NSOTMS>2.0.CO;2, 1986.

Zhang, D.-L., Gao, K., and Parsons, D. B.: Numerical simulation of an intense squall line during 10-11 June 1985 PRE-STORM. Part I: Model verification, *Mon. Wea. Rev.*, 117, 960-994, https://doi.org/10.1175/1520-0493(1989)117,0960:NSOAIS.2.0.CO;2, 1989.

https://doi.org/10.5194/essd-2024-589
Preprint. Discussion started: 30 January 2025

Figures

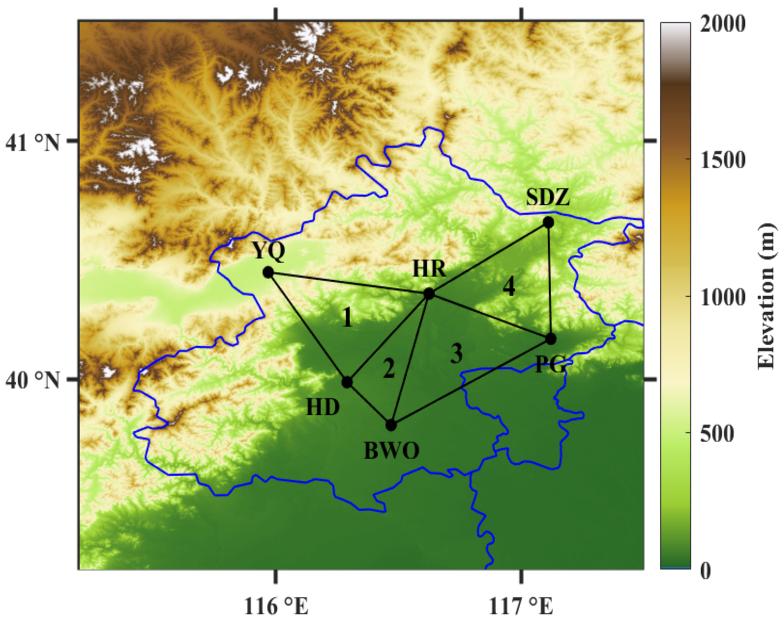

Figure 1. Locations of the six mesonet radar wind profiler (RWP) stations, which are deployed at Huairou (HR; 40.36°N, 116.63°E), Yanqing (YQ; 40.45°N, 115.97°E), Shangdianzi (SDZ; 40.66°N, 117.11°E), Pinggu (PG; 40.17°N, 117.12°E), Haidian (HD; 39.98°N, 116.28°E), and the Beijing Weather Observatory (BWO; 39.79°N, 116.47°E). The blue line denotes the administrative boundaries at the provincial level. Four black triangles with number denote the regions used to calculate the horizontal divergence and vertical vorticity with the triangle method.

https://doi.org/10.5194/essd-2024-589
Preprint. Discussion started: 30 January 2025

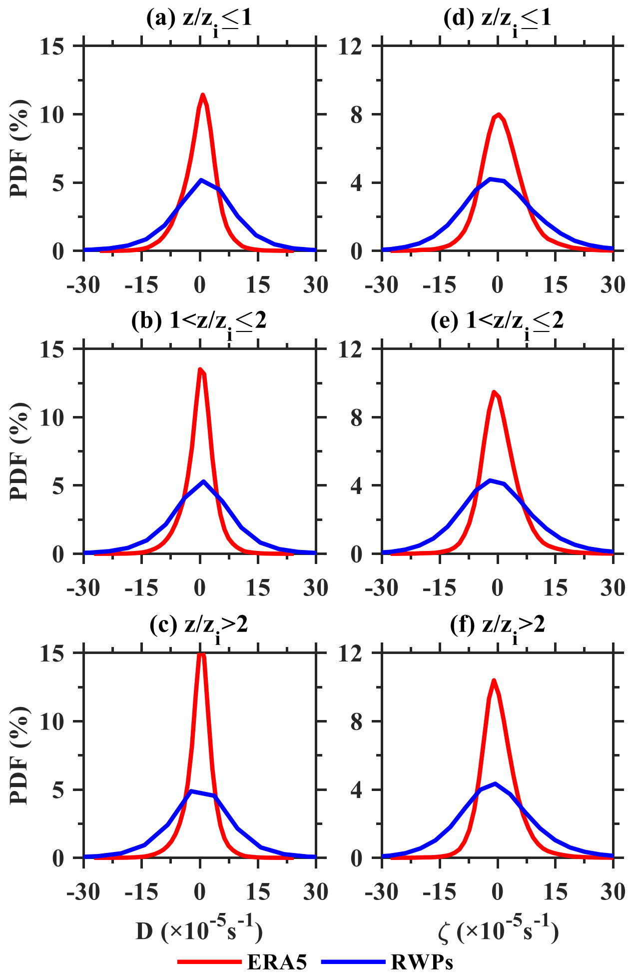

491

492 **Figure 2.** The probability density function (PDF) of horizontal divergence (D) estimated from the measurements of RWPs mesonet (blue line) and ERA5 reanalysis (red line) at the height of (a) $z/z_i \leq 1$, (b) $1<z/z_i \leq 2$, and (c) $z/z_i>2$; (d) –(f) the same as (a)-(c) but for the PDF of vertical vorticity (ζ).

496

497

https://doi.org/10.5194/essd-2024-589
Preprint. Discussion started: 30 January 2025

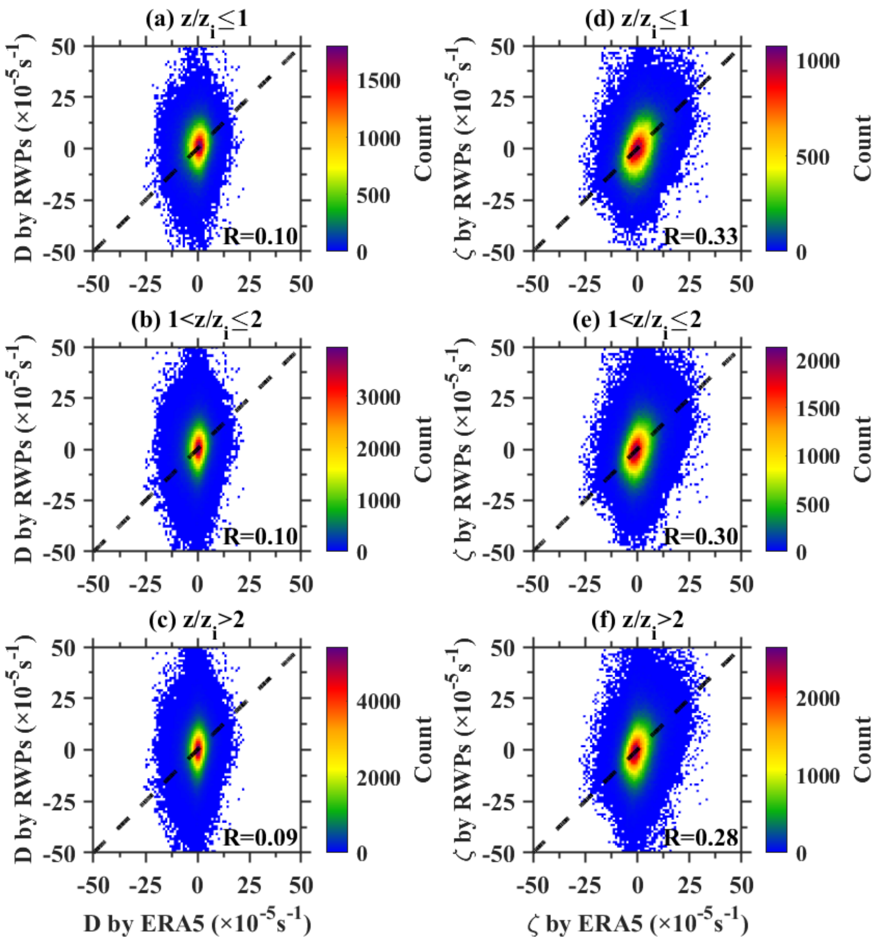

Figure 3. Scatterplots of the horizontal divergence (D) from the measurements of RWPs mesonet versus ERA5 reanalysis at the heights of (a) $z/z_i \leq 1$, (b) $1 < z/z_i \leq 2$, and (c) $z/z_i > 2$ with the 1:1 line shown as black-dashed lines, respectively. The color bar indicates the counts of data points. (d)-(f) the same as (a)-(c) but for the vertical vorticity (ζ).

https://doi.org/10.5194/essd-2024-589
Preprint. Discussion started: 30 January 2025

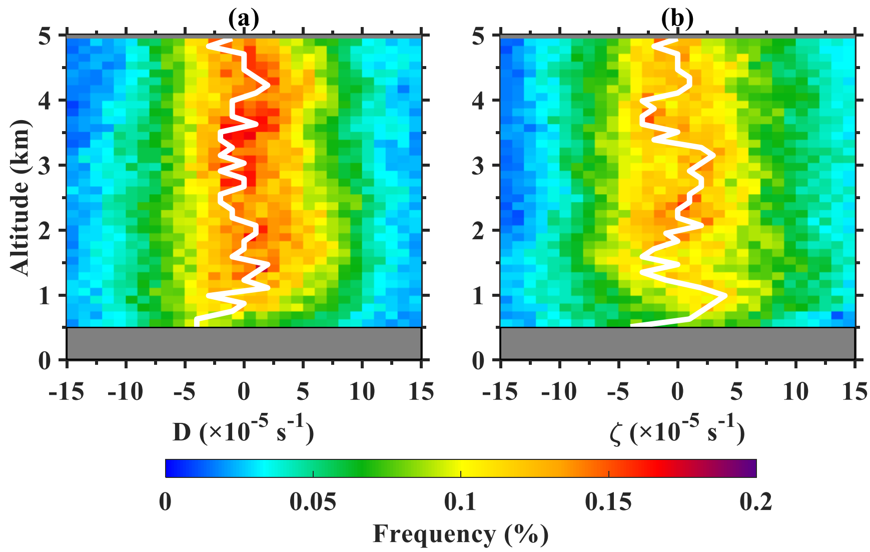

Figure 4. Normalized contoured frequency by altitude (NCFAD) for the horizontal divergence and vertical vorticity between 0.51-4.95 km AMSL as calculated by the RWP mesonet measurements preceding all the rainfall events of 2023 in BMR. Note that the white line represents the profile of maximum frequency distribution. Gray layer is not analyzed due to the error of wind measurements.

https://doi.org/10.5194/essd-2024-589
Preprint. Discussion started: 30 January 2025

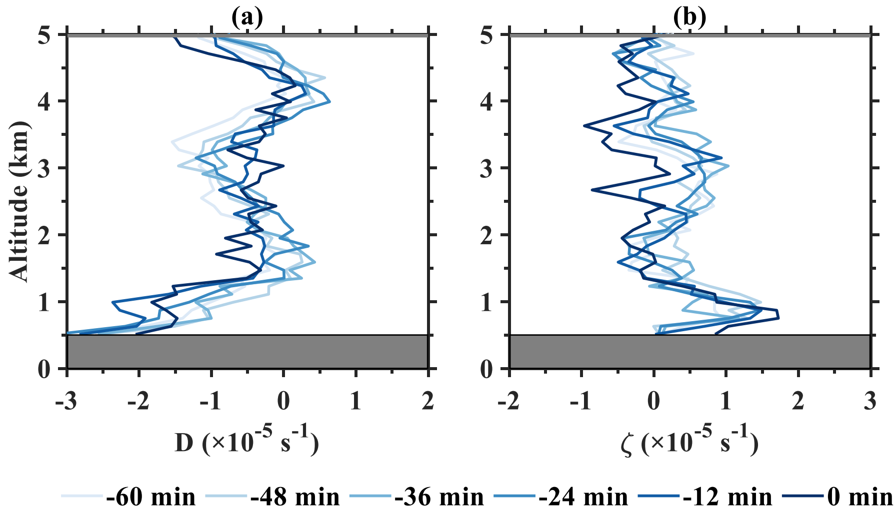

Figure 5. Evolution of the profiles of horizontal divergence (a) and vertical vorticity (b) between 0.51–4.95 km AMSL averaged over 12 minutes, which are calculated from the RWP mesonet (blue line) in the BMR within 1-hour before the onset of rainfall events in 2023. The lowest atmospheric layer shaded in grey is not analyzed due to the error of wind measurements from RWP.